PAPER

Electronic structure and reactivity of a biradical cluster: $Sc_3O_6^-$

Yan-Xia Zhao,[ac] Jin-Yun Yuan,[bc] Xun-Lei Ding,[a] Sheng-Gui He*[a] and
Wei-Jun Zheng*[b]

The $Sc_3O_6^-$ cluster anions were produced by laser ablation and studied by reaction with *n*-butane in a fast flow reactor and by photoelectron spectroscopy. The reactivity experiments indicated that one $Sc_3O_6^-$ cluster can activate two *n*-butane molecules consecutively with rate constants on the order of 10^{-10} cm^3 molecule^{-1} s^{-1} under near room-temperature conditions, suggesting that the even-electron system $Sc_3O_6^-$ has a highly reactive electronic structure. The photoelectron spectroscopy determined a high vertical detachment energy (VDE) of 5.63 ± 0.08 eV for the $Sc_3O_6^-$ cluster. Density functional computations indicated that the lowest energy isomer of $Sc_3O_6^-$ is an oxygen-centered biradical with a high VDE and is highly reactive toward *n*-butane, which is in good agreement with the experiments. The $Sc_3O_6^-$ cluster may serve as an ideal model system to provide insight into the real-life chemistry involved with the coupled $O^{-\bullet} \cdots O^{-\bullet}$ dimers over the surfaces of metal oxide catalysts.

1. Introduction

Biradical species that possess two weakly interacting unpaired electrons individually associated with different atomic centers (such as C, N, and O) are important intermediates in organic reactions, biological and photosynthetic processes.[1–4] Experimental methods such as electron spin resonance and photoelectron spectroscopy in combination with theoretical calculations are widely employed to identify the biradicals.[1–5] Oxygen-centered radicals $O^{-\bullet}$ are important reactive species over metal oxide catalysts[6–10] and it was suggested that two coupled $O^{-\bullet}$ centers can form a dimer species $O^{-\bullet} \cdots O^{-\bullet}$ (biradical).[11] However, due to the heterogeneity of isolated $O^{-\bullet}$ sites and the possible transition of a pair of $O^{-\bullet}$ to O_2^{2-}, it is difficult to characterize the $O^{-\bullet}$ dimers and the nature of such species remains poorly understood.[11]

In order to understand the structure and reactivity of reactive centers over metal oxide surfaces, metal oxide clusters are ideal model systems that can be studied under isolated, controlled, and reproducible conditions.[12–16] A lot of metal oxide clusters[17–38] were identified to have one $O^{-\bullet}$ center. To the

best of our knowledge, for metal oxide systems, only WO_4,[39] $Ti_3VO_{10}^-$,[40] and M_2O_6 (M = Nb, Ta)[41] were suggested to have two $O^{-\bullet}$ centers while the reactivity of such biradicals is unclear. Here, time of flight (TOF) mass spectrometry, anion photoelectron spectroscopy (PES), and density functional theory (DFT) calculations are employed to characterize the electronic structure and reactivity of a novel oxygen-centered biradical cluster $Sc_3O_6^-$. Note that bulk scandium oxides are used as catalytic promoters and/or supports in dehydration of 1,3-diols and 1-4-diols to produce unsaturated alcohols[42,43] and selective reduction of nitric oxide with methane.[44] Study of scandium oxide clusters may provide molecular level insights into the related heterogeneous catalytic systems. Matrix isolation infrared spectroscopy, photoelectron spectroscopy, and mass spectrometry have been employed to study the electronic structure and reactivity of small scandium oxide systems $(ScO_n^{0,\pm1})$[45–50] while the investigation of larger ones $Sc_mO_n^q$ (m > 1) is quite rare and only theoretical studies have been conducted.[51–53]

It should be pointed out that the reactivity of metal oxide cluster anions[30,54–58] toward hydrocarbon molecules has been much less studied in comparison with the extensively studied cluster cations. This is because the negatively-charged metal oxide clusters were usually identified to be much less reactive than the corresponding positively-charged ones. For example, $(V_2O_5)_{1–2}O^-$[54–56] and $(ZrO_2)_{1–4}O^-$[30] display association or minor oxygen atom transfer channels with unsaturated hydrocarbon molecules (such as C_2H_2, C_2H_4), in contrast to the efficient oxygen atom transfer processes in the reactions of $(V_2O_5)_{1–3}^+$[27,54] as well as $(ZrO_2)_{1–5}^+$[28] with these molecules. Therefore, it is desirable to identify metal oxide anions with high oxidative reactivity to enrich the chemistry of gas phase clusters.

[a] *Beijing National Laboratory for Molecular Sciences (BNLMS), State Key Laboratory for Structural Chemistry of Unstable and Stable Species, Institute of Chemistry, Chinese Academy of Sciences, Beijing 100190, People's Republic of China.*
E-mail: shengguihe@iccas.ac.cn or zhengwj@iccas.ac.cn;
Fax: +86-10-62559373;
Tel: +86-10-62536990 or +86-10-62635054
[b] *Beijing National Laboratory for Molecular Sciences (BNLMS), State Key Laboratory of Molecular Reaction Dynamics, Institute of Chemistry, Chinese Academy of Sciences, Beijing 100190, People's Republic of China*
[c] *Graduate School of Chinese Academy of Sciences, Beijing 100039, People's Republic of China*

2. Methods

2.1 Experimental methods

Reactions of scandium oxide anions with butane were investigated by time-of-flight mass spectrometry. The experimental setup for a pulsed laser ablation/supersonic nozzle coupled with a fast flow reactor was described in detail in previous publications.[33,59,60] Only a brief outline of the experiment is given below. The $Sc_mO_n^-$ clusters were generated by laser ablation of a rotating and translating scandium metal disk in the presence of about 0.3% N_2O seeded in the helium (99.99% purity) carrier gas with a backing pressure of 5 atm. A 532 nm (second harmonic of Nd^{3+} : YAG) laser with an energy of 5–8 mJ per pulse and a repetition rate of 10 Hz rate was used. The gas was controlled by a pulsed valve (General Valve, Series 9). In order to eliminate the water impurity that often occurs in the cluster distribution, the prepared gas mixture (N_2O/He, denoted as *cluster generation gas*) was passed through a 10 m long copper tube coil at low temperature ($T = 173$ K) before entering into the pulsed valve. Similar treatment ($T = 263$ K) was also applied in the use of the reactant gases (see below). The generated $Sc_mO_n^-$ anions were expanded and reacted with reactant gases (C_4H_{10}/C_4D_{10}) in a fast flow reactor (6 mm diameter × 60 mm length). The reactant gases with backing pressures of 4–20 kPa were pulsed into the reactor 20 mm downstream from the exit of the narrow cluster formation channel by a second pulsed valve (General Valve, Series 9). The instantaneous total gas pressure in the fast flow reactor was estimated to be around 300 Pa at $T = 350$ K. The cluster vibrational temperature was assumed to be close to the carrier gas temperature which is around 300–400 K considering that the gas can be heated during the process of laser ablation. After reacting in the fast flow reactor, the reactant and product ions exiting from the reactor were skimmed (3 mm diameter) into a vacuum system of a time of flight mass spectrometer (TOF-MS) for mass and intensity measurements. Ion signals were detected by a dual micro-channel plate detector and recorded with a digital oscilloscope (LeCroy WaveSurfer 62Xs) by averaging 500–1000 traces of independent mass spectra (each corresponds to one laser shot). The uncertainty of the reported relative ion signals is about 10%. The mass resolution is about 400–500 ($M/\Delta M$) with the current experimental setup.

To further understand the cluster electronic structure and to provide useful data to gauge the validity of theoretical methods (see below) on scandium oxides, photoelectron spectra of selected $Sc_mO_n^-$ clusters were obtained with a separated vacuum system while the cluster generation was the same as that for the cluster reactivity study (see above). In order to take a photoelectron spectrum, the anions of interest were selected by a mass gate, decelerated by a momentum decelerator, and crossed with the beam of a 266 nm laser (fourth harmonic of Nd^{3+} : YAG) and (or) 193 nm excimer laser (MPB PSX-100) at the photodetachment region of our apparatus which has been described elsewhere.[61] The electrons from photodetachment were energy analyzed by the magnetic-bottle photoelectron spectrometer, which is composed of a permanent magnet located 6 mm below the photodetachment

region, a 2.2 m flight tube surrounded by a solenoid covered with two layers of μ-metal, and a MCP detector. The electric current applied to the solenoid was about 1 A, which produces a magnetic field of ~10 gauss at the center of the flight tube in our case. The resolution of the magnetic-bottle photoelectron spectrometer was ~40 meV at electron kinetic energy of ~1 eV. The photoelectron spectra were calibrated with known spectra of Cu^- and Au^-.[62,63] In this work, photoelectron signals were amplified by a broadband amplifier, digitized with a digital card, and monitored with a laboratory computer. The background noise of the photoelectron spectra was subtracted shot by shot.

2.2 Computational methods

The hybrid B3LYP exchange-correlation functional[64–66] in combination with all-electron polarized triple-ζ valence basis sets (TZVP)[67] were used for Sc, O, C, and H atoms to study the structures of $Sc_3O_{5,6}^-$ clusters and reaction mechanisms of $Sc_3O_6^- + C_4H_{10}$, $Sc_3O_6H^- + C_4H_{10}$, and $Sc_2O_4^- + C_4H_{10}$. The combination of B3LYP/TZVP was tested to give a good prediction for the bond distance, bond strength, and adiabatic ionization and electron affinity energies of the ScO diatomic molecule in our previous study.[37] Meanwhile, the B3LYP/TZVP was also tested to well reproduce the energetics of various main group species including O_2 and small hydrocarbon molecules.[25,26,68] To obtain the lowest energy structures of $Sc_3O_{5,6}^-$, the geometry optimizations were performed starting from a high number of initial structures based on chemical intuitions. All possible spin multiplicities for each geometry were also tested to find the most stable electronic state. All structures presented in this paper were fully optimized and vibrational frequency analysis was performed to ensure that the optimized geometries are minima.

The reaction mechanism calculations involved geometry optimizations of reaction intermediates and transition states (TSs) through which the intermediates transfer to each other. The TS optimizations were performed by using the Berny algorithm.[69] The initial guess structure of the TS species was obtained through relaxed potential energy surface scans using an appropriate internal coordinate. Vibrational frequency calculations were performed to check that reaction intermediates and TS species have zero and one imaginary frequency, respectively. Intrinsic reaction coordinate (IRC)[70,71] calculations were also performed so that a TS connects two appropriate local minima in the reaction pathways. Test calculations indicated that basis set superposition error (BSSE)[72,73] is negligible, so the BSSE was not taken into consideration. The calculated energies reported in this study are the relative zero-point vibration corrected (ΔH_{0K}) and Gibbs free energies (ΔG_{298K}).

The vertical electron detachment energies (VDEs) for the anions $Sc_3O_5^-$ and $Sc_3O_6^-$ are also calculated employing DFT. Both the hybrid functionals (B3LYP,[64–66] B3P86,[65] B1B95,[74] PBE1PBE,[75] B3PW91,[65] O3LYP,[76] BHLYP,[77] B1LYP)[78] and pure GGA functionals (BPW91,[64,79] BLYP,[64,80] PBE,[75,81] BP86)[64,82] in combination with TZVP basis set were tested. To further investigate the reliability of the theoretical methods, the VDEs of ScO^- and ScO_2^- were

This journal is © the Owner Societies 2011

Phys. Chem. Chem. Phys., 2011, **13**, 10084–10090 | 10085

also calculated with some representative functionals and compared with available experimental data. In addition, a larger basis set aug-cc-pVTZ[83,84] was also tested to acquire the basis set effect. Further U/UCCSD(T)[85,86] single point energy calculations were performed with a TZVP basis set for selected cases. All of the theoretical calculations were carried out with the Gaussian 03 program.[87]

3. Results and discussion

3.1 Reactions of $Sc_mO_n^-$ clusters with *n*-butane

The TOF mass spectra for reactions of $Sc_mO_n^-$ ($m = 1$–3) with *n*-butane (C_4H_{10}) in the fast flow reactor under near room-temperature conditions are shown in Fig. 1. The spectra suggest that each of $Sc_2O_{4,5,8}^-$ and $Sc_2O_4N_2O^-$ clusters with odd number of electrons can abstract one hydrogen atom from *n*-butane because $Sc_2O_{4,5,8}H^-$ ($Sc_2O_{4,5,8}D^-$) and $Sc_2O_4N_2OH^-$ ($Sc_2O_4N_2OD^-$) are observed upon the reactions with C_4H_{10} (C_4D_{10}). A previous DFT study[37] indicated that $Sc_2O_4^-$ has a reactive $O^{-\bullet}$ center which should be responsible for the C–H activation[17–24,32–38,88,89] of C_4H_{10}. The experiments imply that the $O^{-\bullet}$ centers may also exist in the *odd-electron* systems $Sc_2O_{5,8}^-$ and $Sc_2O_4N_2O^-$, which may be verified by further theoretical studies.

The most interesting result in Fig. 1 (see the right side) is that the reactions of the *even-electron* cluster $Sc_3O_6^-$ with C_4H_{10} (C_4D_{10}) molecules generate $Sc_3O_6H^-$ ($Sc_3O_6D^-$) and $Sc_3O_6H_2^-$ ($Sc_3O_6D_2^-$). When higher pressure of C_4H_{10} (see Fig. 1b and c) is used in the reactor, the signal of $Sc_3O_6H^-$ decreases while that of $Sc_3O_6H_2^-$ increases, indicating that $Sc_3O_6H_2^-$ is produced from the secondary reaction $Sc_3O_6H^-$ + C_4H_{10} rather than from $Sc_3O_6^-$ + C_4H_{10} directly. Although the *even-electron* cluster $Sc_3O_5^-$ is also produced in the cluster source (Fig. 1a), there is no indication for the production of $Sc_3O_5H^-$ or $Sc_3O_5H_2^-$ after the reaction (Fig. 1b and c) under the same experimental condition, suggesting that $Sc_3O_5^-$ is inert toward C_4H_{10}. Note that a weak peak (217 amu, marked with asterisk in Fig. 1a) next to
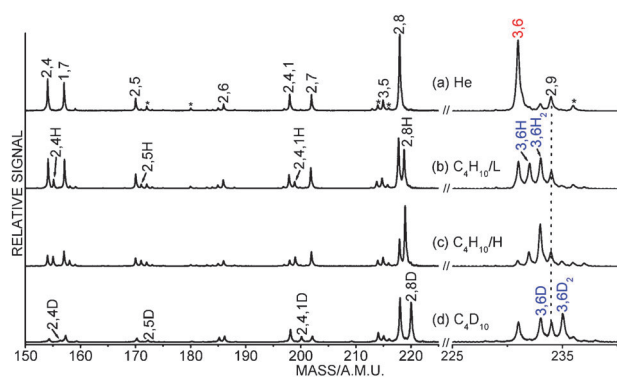
$Sc_3O_5^-$ (215 amu) can be assigned as a N_2 containing cluster $ScO_8N_2O^-$.

The first order rate constant (k_1) in the fast flow reactor can be estimated by $I = I_0 \exp(-k_1 \rho l/v)$, in which I and I_0 are signal magnitudes of the clusters in the presence and absence of reagent gas (C_4H_{10}), respectively; ρ is the molecular density of reactant gas (the method to calculate ρ has been described in ref. 90); l is the effective length of the reactor (~ 60 mm); and v is the cluster beam velocity (~ 1 km s^{-1}). The estimated $k_1(Sc_3O_6^- + C_4H_{10})$ is $(2.9 \pm 1.5) \times 10^{-10}$ cm^3 molecule^{-1} s^{-1}. The reaction efficiency (Φ) can be defined as $k_1(Sc_3O_6^- + C_4H_{10})/k_c(Sc_3O_6^- + C_4H_{10})$, in which $k_c(Sc_3O_6^- + C_4H_{10})$ is the rate of collision between $Sc_3O_6^-$ and C_4H_{10}. The Φ value is calculated to be 0.29 by assuming effective diameters of $Sc_3O_6^-$ and C_4H_{10} as 0.47 and 0.66 nm, respectively. The value of kinetic isotope effect (KIE) $k_1(Sc_3O_6^- + C_4H_{10})/k_1(Sc_3O_6^- + C_4D_{10})$ is determined to be 1.9 ± 0.4. It is noticeable that only a few examples of alkane activation by metal oxide anions have been reported.[91] Our recent experiments[56,57,92,93] indicated that $(ZrO_2)_{2,3}O^-$, $Zr_2O_8^-$, $(V_2O_5)_{1,2}O^-$, and $(V_2O_5)(SiO_2)_{1-4}O^-$ can activate C_4H_{10} with rate constants in the magnitude of 10^{-12}–10^{-11} cm^3 molecule^{-1} s^{-1}, which are significantly smaller than $k_1(Sc_3O_6^- + C_4H_{10})$. It implies that the even-electron system $Sc_3O_6^-$ has a highly reactive (open-shell) electronic structure.

3.2 Photoelectron spectroscopy and electronic structure of the $Sc_3O_6^-$ cluster

The photoelectron spectra in Fig. 2 indicate that the $Sc_3O_6^-$ cluster has a high vertical electron detachment energy (VDE) of 5.63 ± 0.08 eV, which is much larger than the VDE of $Sc_3O_5^-$ (3.15 ± 0.08 eV).

The B3LYP calculated isomers for $Sc_3O_6^-$ are shown in Fig. 3a. It can be seen that the lowest energy isomer (I01) of $Sc_3O_6^-$ is a triplet (C_s, $^3A''$) with two identical Sc–O_t terminal bonds of which the lengths (204 pm) are significantly longer than that of diatomic ScO (167 pm by B3LYP). As shown in Fig. 3b, the two singly occupied molecule orbitals (SOMOs) ψ_a and ψ_b in I01 are essentially the 2p orbitals of the two O_t atoms. Each of the O_t atoms has Mulliken atomic spin densities close to one unit μ_B (Fig. 3b, $|\psi|^2$). Note that Fock exchange (FE) in the hybrid B3LYP tends to localize the unpaired electrons,[94] while test calculations by BLYP functional (without the FE) also predict highly localized unpaired electrons in $Sc_3O_6^-$ (I01): each of the two O_t atoms has spin density values of 0.94 μ_B. The two O_t atoms in $Sc_3O_6^-$

Fig. 1 TOF mass spectra for reactions of $Sc_mO_n^-$ with He (a, for reference), 0.3 Pa C_4H_{10} (b), 0.6 Pa C_4H_{10} (c), and 0.6 Pa C_4D_{10} (d). Numbers *m,n* denote $Sc_mO_n^-$ and *m,n*X denote $Sc_mO_nX^-$ (X = H, D, H_2, or D_2). Note that N_2O was used as oxygen source in generation of the clusters and some N_2-containing clusters (marked with asterisks) such as $Sc_2O_4N_2O^-$ (marked as 2,4,1) are present.
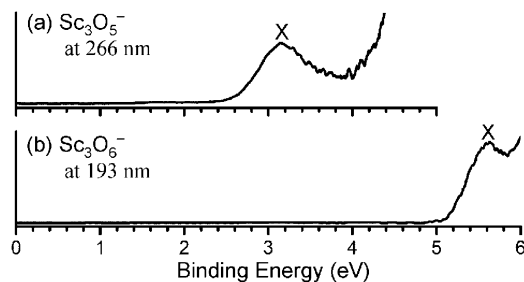

Fig. 2 Photoelectron spectra of $Sc_3O_5^-$ at 266 nm and $Sc_3O_6^-$ at 193 nm.
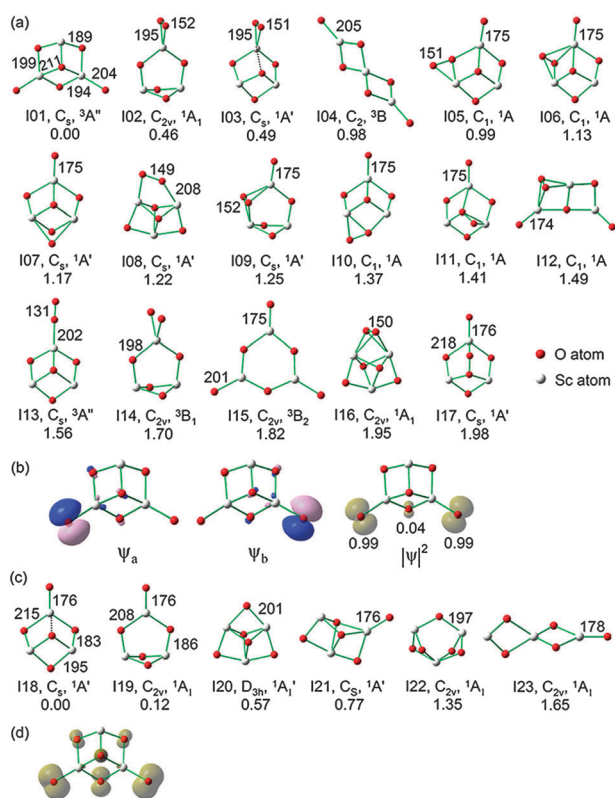
Fig. 3 (a) B3LYP optimized isomeric structures of $Sc_3O_6^-$; (b) profiles of the two singly occupied molecular orbitals and the distributions of spin densities for isomer I01; (c) B3LYP optimized isomeric structures of $Sc_3O_5^-$; and (d) profile of spin density distribution for neutral Sc_3O_6 in quartet state. Some Sc–O and O–O distances in pm are given. The relative energies in eV are given below the labels for point group and electronic symmetries. The spin density values in μ_B are given in (b) for three related oxygen atoms.

(I01) can be considered as adsorbed $O^{-\bullet}$ radicals and $Sc_3O_6^-$ (I01) is an oxygen-centered biradical. The energy difference between the open shell singlet (geometry is optimized and very close to that of the triplet) and the triplet for the I01 isomer is only 5.4×10^{-5} eV under B3LYP calculations. This is in agreement with the disjoint character of ψ_a and ψ_b in Fig. 3b: the Coulomb repulsion of the two unpaired electrons in the open shell singlet is not significantly larger than that in the triplet. Note that the distance between the two $O^{-\bullet}$ centers in I01 is 637 pm. The closed shell singlet is much higher in energy (by 2.24 eV) than the triplet or open shell singlet for the I01 isomer. Each of the two low-lying energy isomers of $Sc_3O_6^-$

(I02 and I03 in Fig. 3a) has a η^2-O_2 moiety and is significantly unstable (>0.4 eV) than I01 by the B3LYP.

The DFT calculated VDE values for $Sc_3O_6^-$ are listed in Table 1. Meanwhile, in order to gauge the accuracy of the adopted methods, the VDEs for $ScO_{1,2}^-$ and $Sc_3O_5^-$ by the DFT are also listed and compared with available experimental data.[50] The B3LYP calculated low-lying energy isomers for $Sc_3O_5^-$ are summarized in Fig. 3c. The lowest energy isomer of $Sc_3O_5^-$ (I18) is a closed shell singlet and the $Sc–O_t$ terminal bond in I18 (176 pm, $Sc=O$ double bond) is significantly shorter than those in I01 (204 pm). As a result, there is no reactive oxygen center $O^{-\bullet}$ in $Sc_3O_5^-$ (I18). Note that appearance of $O^{-\bullet}$ in $Sc_3O_5^-$ (I18) would require excitation of the valence electrons in O 2p orbital(s) to the Sc 3d orbital(s) [for example: $^1Sc_3O_5^- + h\nu \rightarrow Sc_3O_5^-$ (singlet or triplet, with electron–hole pair)] or to vacuum (for example: $^1Sc_3O_5^- + h\nu \rightarrow {}^2Sc_3O_5 + e^-$, ground state of $^2Sc_3O_5$ has a $O^{-\bullet}$ center).[37]

Table 1 shows that the B3LYP functional with a relatively large basis set (aug-cc-pVTZ) reproduces the VDE values of $ScO_{1,2}^-$ [50] and $Sc_3O_5^-$ very well while the high VDE of $Sc_3O_6^-$ [if interpreted as $^3Sc_3O_6^-$ (I01) $\rightarrow {}^4Sc_3O_6 + e^-$] is under-estimated by about 10%. A lot of other functionals including B3P86, B1B95, PBE1PBE, B3PW91, O3LYP, BHLYP, and B1LYP; and BPW91, BLYP, PBE, and BP86 have also been tested and the representative results by B3P86 and BPW91 are also listed in Table 1. Compared with B3LYP, these alternative functionals generally give less good results for the VDEs of $ScO_{1,2}^-$ and $Sc_3O_5^-$ while one of them (B3P86) predicts a good match (5.59 eV versus 5.63 eV) for the VDE of $Sc_3O_6^-$. More expensive CCSD(T)/TZVP single point energy calculations at B3LYP/TZVP and B3P86/TZVP optimized $Sc_3O_6^-$ (I01) structures predict the VDE values of 5.17 and 5.19 eV, respectively.

The B3LYP/aug-cc-pVTZ predicts that the VDEs of $Sc_3O_6^-$ isomers I02 and I03 (Fig. 3a) are 3.10 and 2.97 eV, respectively, which are too small compared with the experimental value of 5.63 ± 0.08 eV. This discards the possibility that these low-lying energy isomers with unbroken O–O bonds (η^2-O_2) are the ground state of $Sc_3O_6^-$. The second VDE of the I01 ($^3Sc_3O_6^- \rightarrow {}^2Sc_3O_6 + e^-$) by B3LYP/aug-cc-pVTZ is 5.28 eV [5.21 eV by CCSD(T)/TZVP single point calculations], which is a little higher than the first VDE ($^3Sc_3O_6^- \rightarrow {}^4Sc_3O_6 + e^-$). This means that the broad X band in Fig. 2b is possibly due to the above two channels of electron detachments. Wang et al. have identified that many oxygen-rich transition-metal clusters possess high VDEs (like $Sc_3O_6^-$ in Fig. 2a), which is a consequence of delocalization of the extra electron over

Table 1 Experimental and theoretical vertical electron detachment energies (eV) of $ScO_{1,2}^-$ and $Sc_3O_{5,6}^-$ clusters
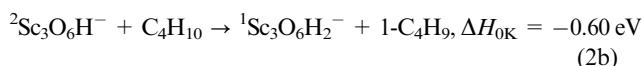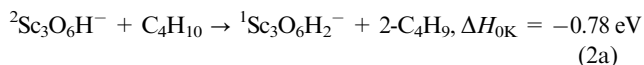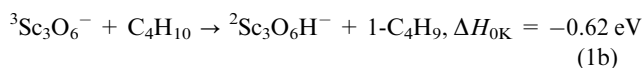
		B3LYP	B3P86	BPW91	CCSD(T)	Expt.
$^1ScO^-$	TZVP	1.09	1.52	0.90		1.35(2)[50]
	aug-cc-pVTZ	1.28	1.68	1.08		
$^1ScO_2^-$	TZVP	1.88	2.45	1.65		2.32(2)[50]
	aug-cc-pVTZ	2.28	2.77	2.05		
$^1Sc_3O_5^-$	TZVP	3.06	3.64	2.96		3.15(8)
	aug-cc-pVTZ	3.14	3.65	3.09		
$^3Sc_3O_6^-$ (I01)	TZVP	4.97	5.57	4.28	5.17	5.63(8)
	aug-cc-pVTZ	5.05	5.59	6.52		

This journal is © the Owner Societies 2011

Phys. Chem. Chem. Phys., 2011, 13, 10084–10090 | 10087

several O centers.[39] The spin density distribution of the neutral Sc_3O_6 (I01, quartet state) is shown in Fig. 3d (see also Fig. 3b for $|\psi|^2$). It indicates that the vertical electron excitation $^3Sc_3O_6^-$ (I01) $\rightarrow$ $^4Sc_3O_6$ + e^- involves all of the six oxygen atoms: the extra electron to be excited is highly delocalized.

It can be seen that there are reasonably good matches between the B3LYP calculations and the experiments for the photoelectron spectra of $Sc_3O_6^-$ as well as those of $ScO_{1,2}^-$ and $Sc_3O_5^-$. Meanwhile, the cluster reactivity experiments (Fig. 1) suggest a highly reactive open-shell electronic structure for $Sc_3O_6^-$. As a result, we conclude that the lowest energy isomer (I01, Fig. 3a) of $Sc_3O_6^-$ by the B3LYP is the ground state, i.e., the PES and reactivity of $Sc_3O_6^-$ clusters in experiments are due to oxygen-centered biradical species.

3.3 Reaction mechanisms of $Sc_3O_6^-$ + n-C_4H_{10}

To understand the mechanistic details of hydrogen atom abstraction from C_4H_{10} by $Sc_3O_6^-$ and $Sc_3O_6H^-$, reactions (1) and (2) below have been studied by B3LYP/TZVP calculations.

$$^3Sc_3O_6^- + C_4H_{10} \rightarrow {}^2Sc_3O_6H^- + 2\text{-}C_4H_9, \Delta H_{0K} = -0.80 \text{ eV} \tag{1a}$$

$$^3Sc_3O_6^- + C_4H_{10} \rightarrow {}^2Sc_3O_6H^- + 1\text{-}C_4H_9, \Delta H_{0K} = -0.62 \text{ eV} \tag{1b}$$

$$^2Sc_3O_6H^- + C_4H_{10} \rightarrow {}^1Sc_3O_6H_2^- + 2\text{-}C_4H_9, \Delta H_{0K} = -0.78 \text{ eV} \tag{2a}$$

$$^2Sc_3O_6H^- + C_4H_{10} \rightarrow {}^1Sc_3O_6H_2^- + 1\text{-}C_4H_9, \Delta H_{0K} = -0.60 \text{ eV} \tag{2b}$$
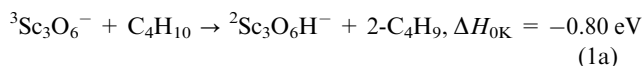
The potential energy profiles of reactions (1) and (2) are shown in Fig. 4. The structures of the related reaction intermediates and transition states are plotted in Fig. 5. As to reaction (1a), in the encounter complex (IM1), two hydrogen atoms weakly interact with one of the $O^{-\bullet}$ centers. Then the reaction proceeds by a transition state (TS1) for C–H activation and H atom transfer (IM1→TS1→IM2). If the zero-point energy

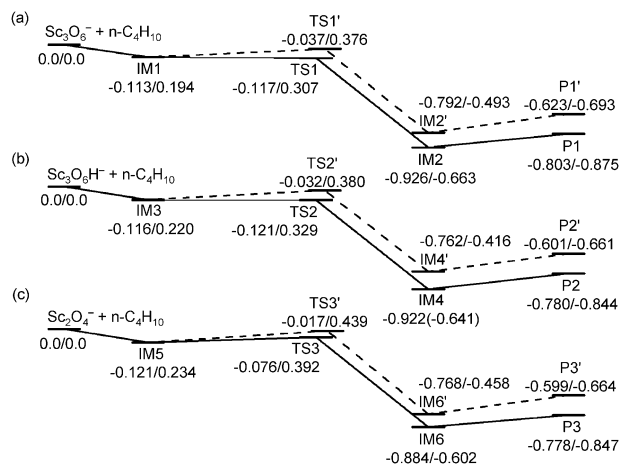**Fig. 4** B3LYP calculated potential energy profiles for (a) $^3Sc_3O_6^-$ + n-C_4H_{10}; (b) $^2Sc_3O_6H^-$ + n-C_4H_{10}; and (c) $^2Sc_2O_4^-$ + n-C_4H_{10}. The relative $\Delta H_{0K}/\Delta G_{298K}$ values in eV are given. See Fig. 5 for the structures of the reactants, products, reaction intermediates, and transition states.
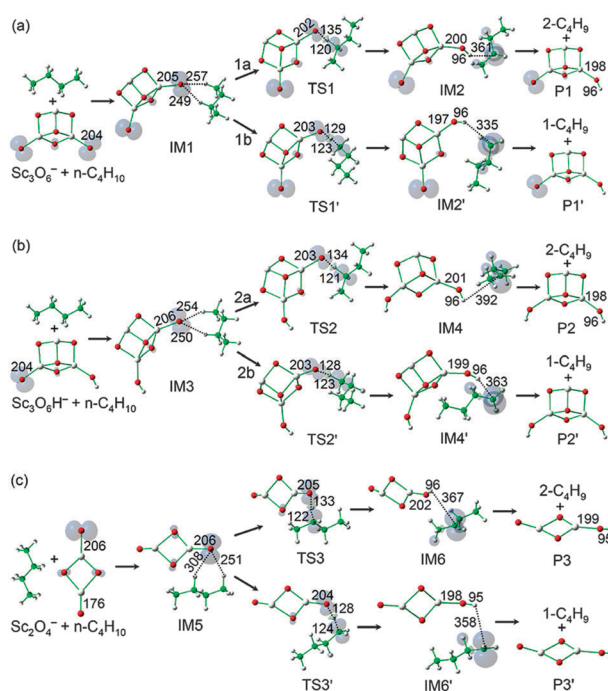
Fig. 5 B3LYP optimized structures of the reactants, products, reaction intermediates, and transition states for (a) $^3Sc_3O_6^-$ + n-C_4H_{10}; (b) $^2Sc_3O_6H^-$ + n-C_4H_{10}; and (c) $^2Sc_2O_4^-$ + n-C_4H_{10} in Fig. 4. Some critical distances in pm are given.

(ZPE) correction is not taken into account, TS1 is 0.14 eV higher in energy than IM1. The TS1 is below IM1 by 0.004 eV when the ZPE is included. Reaction (1a) is driven by highly favorable thermodynamics after the H atom transfer. Reaction (1b) needs to overcome relatively higher activation barrier (0.076 eV) than reaction (1a) does, which correlates with the relative thermodynamics. One $O^{-\bullet}$ center is left in $Sc_3O_6H^-$ (see the Sc_3O_6H moiety of IM2), so the mechanisms of reactions (2a) and (2b) are very similar to those of (1a) and (1b), respectively. Likewise, reaction (2b) is less favorable than (2a) thermodynamically and kinetically. To conclude, the activation of methyl group in C_4H_{10} (reactions (1b) and (2b)) is less favorable than that of the methylene group (reactions (1a) and (2a)).

Methane activation is a holy grail in alkane chemistry.[95] To the best of our knowledge, none of the metal oxide cluster anions has been experimentally identified to be able to activate CH_4 at near room-temperature conditions, although many oxide cluster cations are highly reactive with CH_4.[17–24,32–36,88,89] Considering the high reactivity of $Sc_3O_6^-$ toward activation of the C–H bonds in C_4H_{10}, we are interested to estimate a rate constant for methane activation by this cluster. The energy barrier for C–H activation of CH_4 by $Sc_3O_6^-$ is 0.106 eV (ΔH_{0K} value) under B3LYP calculations. The $k_1(Sc_3O_6^-$ + $CH_4)$ may be scaled from $k_1(Sc_3O_6^-$ + $C_4H_{10})$ by a factor of $\exp(-\Delta E_a/k_BT)$, in which ΔE_a is the difference of the C–H activation barrier (0.223 eV) between CH_4 and C_4H_{10}, k_B is the Boltzmann constant, and T is the temperature. For $T = 298$ K, $k_1(Sc_3O_6^-$ + $CH_4)$ is estimated to be 4.87×10^{-14} cm^3 molecule^{-1} s^{-1}, which is larger than $k_1(OH + CH_4) = 7.89 \times 10^{-15}$ cm^3 molecule^{-1} s^{-1}.[96]

10088 | *Phys. Chem. Chem. Phys.*, 2011, **13**, 10084–10090

This journal is © the Owner Societies 2011

This indicates that $Sc_3O_6^-$ may be as reactive as the OH free radical in terms of the methane activation. The room-temperature methane activation by $Sc_3O_6^-$ cluster anions may well be demonstrated if $Sc_3O_6^-$ is trapped and reacted with CH_4 in a reactor with a relatively long period of time.

3.4 Comparison of $Sc_3O_6^-$ with $Sc_2O_4^-$

The DFT calculations indicate that both $Sc_2O_4^-$ (see ref. 37) and $Sc_3O_6^-$ have two terminal oxygen atoms while the former only contains one oxygen radical ($O^{-\bullet}$) and the latter has two oxygen radicals. In our previous studies,[37,38] for oxide clusters $M_xO_y^q$, a value to evaluate the extent of oxygen richness or poorness was defined as $\Delta \equiv 2y - nx + q$, in which n is the number of valence electrons of element M that can be oxidized by oxygen to the $+n$ oxidation state and q ($=0, \pm1$) is the charge number. With our definition, the Δ values of $Sc_2O_4^-$ and $Sc_3O_6^-$ are $+1$ and $+2$, respectively, which is consistent with the detailed DFT results that there is one $O^{-\bullet}$ unit in $Sc_2O_4^-$ while two $O^{-\bullet}$ units in $Sc_3O_6^-$. This also suggests that the $\Delta = +2$ metal oxide clusters are candidates of oxygen-centered bi-radicals if they are not peroxides (like I02 and I03 in Fig. 3a).

The experimentally estimated first order rate constant for $Sc_2O_4^- + C_4H_{10}$ is $(8.0 \pm 1.5) \times 10^{-11}$ cm^3 molecule^{-1} s^{-1}, which is significantly smaller than that for $Sc_3O_6^- + C_4H_{10}$ $(2.9 \pm 1.5) \times 10^{-10}$ cm^3 molecule^{-1} s^{-1}. The DFT results in Fig. 4c and 5c indicate that the C–H (in the methylene group) activation by $Sc_2O_4^-$ (IM5→TS3→IM6) is subject to a small barrier (0.045 eV) while the corresponding steps (IM1→TS1→IM2 and IM3→TS2→IM4, Fig. 4a and b) in $Sc_3O_6^-$ and $Sc_3O_6H^-$ reaction systems are barrierless in terms of the relative enthalpy change (ΔH_{0K}). In the experiments, the encounter complex (such as IM1, IM3, or IM5 in Fig. 5) carries center-of-mass collisional energy E_k and cluster vibrational energy E_{vib}, in which $E_k = 1/2\ \mu v^2$ (μ is the reduced mass of the $Sc_mO_n^-$ cluster with n-C_4H_{10}, $v \approx 1$ km s^{-1}) and E_{vib} can be estimated from the DFT calculations for the vibrational temperature of $T = 350$ K. Given that the reaction intermediates are not in fully thermal equilibrium due to low pressure (~300 Pa) in the fast flow reactor, the excess energy ($E_{exc} = E_k + E_{vib}$) can be used to surmount the Gibbs free energy barrier for the C–H activation. The E_{exc} values for $Sc_3O_6^- \cdots C_4H_{10}$ (IM1) and $Sc_2O_4^- \cdots C_4H_{10}$ (IM5) are 0.62 eV and 0.49 eV, respectively. In addition, the $Sc_3O_6^-$ has two $O^{-\bullet}$ centers while $Sc_2O_4^-$ has only one. All of the above factors (activation barrier, excess energy, and number of active sites) favor a faster reaction of $Sc_3O_6^- + C_4H_{10}$ versus $Sc_2O_4^- + C_4H_{10}$, which is consistent with the experiments.

4. Conclusions

Scandium oxide cluster anions $Sc_mO_n^-$ were generated by laser ablation and reacted with n-C_4H_{10} in a fast flow reactor. Observation of hydrogen atom pickup products $Sc_3O_6H^-$ and $Sc_3O_6H_2^-$ indicated that the even-electron cluster $Sc_3O_6^-$ can abstract two hydrogen atoms from two n-C_4H_{10} molecules consecutively with a rate constant on the order of 10^{-10} cm^3 molecule^{-1} s^{-1} under near room temperature

conditions. The experimentally determined vertical electron detachment energy of $Sc_3O_6^-$ is 5.63 ± 0.08 eV. Further theoretical studies on the geometric structure, vertical detachment energy, and reaction mechanisms confirmed that the ground state of $Sc_3O_6^-$ is an oxygen-centered biradical, which is responsible for the consecutive C–H activations. The identification of the $Sc_3O_6^-$ cluster as a biradical is significant because it may serve as an ideal model system to provide insight into the real-life chemistry involved with the coupled $O^{-\bullet} \cdots O^{-\bullet}$ dimers over the surfaces of metal oxide catalysts. Important mechanistic details such as two state reactivity[97] may be investigated by studying reactions of $Sc_3O_6^-$ with small molecules.[98]

References

1 A. Rajca, *Chem. Rev.*, 1994, **94**, 871.
2 A. Berson, *Acc. Chem. Res.*, 1978, **11**, 446.
3 A. L. Buchachenko and V. L. Berdinskym, *Chem. Rev.*, 2002, **102**, 603.
4 R. Jahjah, A. Gassama, V. Bulach, C. Suzuki, M. Abe, N. Hoffmann, A. Martinez and J.-M. Nuzillard, *Chem.–Eur. J.*, 2010, **16**, 3341.
5 T. Ichino, S. M. Villano, A. J. Gianola, D. J. Goebbert, L. Velarde, A. Sanov, S. J. Blanksby, X. Zhou, D. A. Hrovat, W. T. Borden and W. C. Lineberger, *Angew. Chem., Int. Ed.*, 2009, **48**, 8509.
6 V. A. Shvets and V. B. Kazansky, *J. Catal.*, 1972, **25**, 123.
7 N. I. Lopatkina, V. A. Shvets and V. B. Kazansky, *Kinet. Katal.*, 1978, **19**, 979.
8 R. S. Liu, M. Iwamoto and J. H. Lunsford, *J. Chem. Soc., Chem. Commun.*, 1982, 78.
9 H. F. Liu, R. S. Liu, K. Y. Liew, R. E. Johnson and J. H. Lunsford, *J. Am. Chem. Soc.*, 1984, **106**, 4117.
10 H. Launay, S. Loridant, D. L. Nguyen, A. M. Volodin, J. L. Dubois and J. M. M. Millet, *Catal. Today*, 2007, **128**, 176.
11 M. Che and A. J. Tench, *Adv. Catal.*, 1982, **31**, 77.
12 P. Jena and A. W. Castleman, Jr., *Proc. Natl. Acad. Sci. U. S. A.*, 2006, **103**, 10560.
13 D. Schröder and H. Schwarz, *Proc. Natl. Acad. Sci. U. S. A.*, 2008, **105**, 18114.
14 P. B. Armentrout, *Annu. Rev. Phys. Chem.*, 2001, **52**, 423.
15 R. A. J. O'Hair and G. N. Khairallah, *J. Cluster Sci.*, 2004, **15**, 331.
16 Y. Gong and M. F. Zhou, *Chem. Rev.*, 2009, **109**, 6765.
17 K. K. Irikura and J. L. Beauchamp, *J. Am. Chem. Soc.*, 1989, **111**, 75.
18 D. Schröder, A. Fiedler, J. Hrušák and H. Schwarz, *J. Am. Chem. Soc.*, 1992, **114**, 1215.
19 I. Kretzschmar, A. Fiedler, J. N. Harvey, D. Schröder and H. Schwarz, *J. Phys. Chem. A*, 1997, **101**, 6252.
20 J. N. Harvey, M. Diefenbach, D. Schröder and H. Schwarz, *Int. J. Mass Spectrom.*, 1999, **182/183**, 85.
21 S. Feyel, J. Döbler, D. Schröder, J. Sauer and H. Schwarz, *Angew. Chem., Int. Ed.*, 2006, **45**, 4681.
22 D. Schröder and J. Roithová, *Angew. Chem., Int. Ed.*, 2006, **45**, 5705.
23 S. Feyel, J. Döbler, R. Höckendorf, M. K. Beyer, J. Sauer and H. Schwarz, *Angew. Chem., Int. Ed.*, 2008, **47**, 1946.
24 M. Schlangen and H. Schwarz, *Dalton Trans.*, 2009, 10155.
25 F. Dong, S. Heinbuch, Y. Xie, J. J. Rocca, E. R. Bernstein, Z.-C. Wang, K. Deng and S.-G. He, *J. Am. Chem. Soc.*, 2008, **130**, 1932.

This journal is © the Owner Societies 2011

Phys. Chem. Chem. Phys., 2011, **13**, 10084–10090 | 10089

26 F. Dong, S. Heinbuch, Y. Xie, E. R. Bernstein, J. J. Rocca, Z.-C. Wang, X.-L. Ding and S.-G. He, *J. Am. Chem. Soc.*, 2009, **131**, 1057.

27 D. R. Justes, R. Mitrić, N. A. Moore, V. Bonačić-Koutecky and A. W. Castleman, Jr., *J. Am. Chem. Soc.*, 2003, **125**, 6289.

28 G. E. Johnson, R. Mitrić, E. C. Tyo, V. Bonačić-Kouteck and A. W. Castleman, Jr., *J. Am. Chem. Soc.*, 2008, **130**, 13912.

29 G. E. Johnson, E. C. Tyo and A. W. Castleman, Jr., *Proc. Natl. Acad. Sci. U. S. A.*, 2008, **105**, 18108.

30 G. E. Johnson, R. Mitrić, M. Nössler, E. C. Tyo, V. Bonačić-Kouteck and A. W. Castleman, Jr., *J. Am. Chem. Soc.*, 2009, **131**, 5460.

31 M. Nößler, R. Mitrić, V. Bonačić-Koutecky, G. E. Johnson, E. C. Tyo and A. W. Castleman, Jr., *Angew. Chem., Int. Ed.*, 2010, **49**, 407.

32 Y.-X. Zhao, X.-N. Wu, Z.-C. Wang, S.-G. He and X.-L. Ding, *Chem. Commun.*, 2010, **46**, 1736.

33 X.-N. Wu, Y.-X. Zhao, W. Xue, Z.-C. Wang, S.-G. He and X.-L. Ding, *Phys. Chem. Chem. Phys.*, 2010, **12**, 3984.

34 Z.-C. Wang, X.-N. Wu, Y.-X. Zhao, J.-B. Ma, X.-L. Ding and S.-G. He, *Chem. Phys. Lett.*, 2010, **489**, 25.

35 X.-L. Ding, Y.-X. Zhao, X.-N. Wu, Z.-C. Wang, J.-B. Ma and S.-G. He, *Chem.–Eur. J.*, 2010, **16**, 11463.

36 J.-B. Ma, X.-N. Wu, Y.-X. Zhao, X.-L. Ding and S.-G. He, *Phys. Chem. Chem. Phys.*, 2010, **12**, 12223.

37 Y.-X. Zhao, X.-L. Ding, Y.-P. Ma, Z.-C. Wang and S.-G. He, *Theor. Chem. Acc.*, 2010, **127**, 449.

38 Y.-X. Zhao, X.-N. Wu, J.-B. Ma, S.-G. He and X.-L. Ding, *Phys. Chem. Chem. Phys.*, 2011, **13**, 1925.

39 H.-J. Zhai, B. Kiran, L.-F. Cui, X. Li, D. A. Dixon and L.-S. Wang, *J. Am. Chem. Soc.*, 2004, **126**, 16134.

40 E. Janssens, G. Santambrogio, M. Brümmer, L. Wöste, P. Lievens, J. Sauer, G. Meijer and K. R. Asmis, *Phys. Rev. Lett.*, 2006, **96**, 233401.

41 H.-J. Zhai, X.-H. Zhang, W.-J. Chen, X. Huang and L.-S. Wang, *J. Am. Chem. Soc.*, 2011, **133**, 3085.

42 S. Sato, R. Takahashi, T. Sodesawa, A. Igarashi and H. Inoue, *Appl. Phys. A: Mater. Sci. Process.*, 2007, **328**, 109.

43 S. Sato, R. Takahashi, M. Kobune, H. Inoue, Y. Izawa, H. Ohno and K. Takahashi, *Appl. Phys. A: Mater. Sci. Process.*, 2009, **356**, 64.

44 M. D. Fokema and J. Y. Ying, *Appl. Phys. B: Lasers Opt.*, 1998, **18**, 71.

45 Y. Gong, C.-F. Ding and M.-F. Zhou, *J. Phys. Chem. A*, 2007, **111**, 11572.

46 C. W. Bauschlicher, Jr., M.-F. Zhou, L. Andrews, J. R. T. Johnson, I. Panas, A. Snis and B. O. Roos, *J. Phys. Chem. A*, 1999, **103**, 5463.

47 S.-J. Kim and T. D. Crawford, *J. Phys. Chem. A*, 2004, **108**, 3097.

48 E. P. F. Lee, D. K. W. Mok, F.-T. Chau and J. M. Dyke, *J. Comput. Chem.*, 2008, **30**, 337.

49 D. E. Clemmer, N. Aristov and P. B. Armentrout, *J. Phys. Chem.*, 1993, **97**, 544.

50 H. Wu and L.-S. Wang, *J. Phys. Chem. A*, 1998, **102**, 9129.

51 J. R. T. Johnson and I. Panas, *Chem. Phys.*, 1999, **248**, 161.

52 J.-L. Wang, Y.-B. Wang, G.-F. Wu, X.-Y. Zhang, X.-J. Zhao and M.-L. Yang, *Phys. Chem. Chem. Phys.*, 2009, **11**, 5980.

53 Y.-B. Wang, X.-X. Gong and J.-L. Wang, *Phys. Chem. Chem. Phys.*, 2010, **12**, 2471.

54 K. A. Zemski, D. R. Justes and A. W. Castleman, Jr., *J. Phys. Chem. A*, 2001, **105**, 10237.

55 R. C. Bell and A. W. Castleman, Jr., *J. Phys. Chem. A*, 2002, **106**, 9893.

56 J.-B. Ma, X.-N. Wu, Y.-X. Zhao, S.-G. He and X.-L. Ding, *Acta Phys. Chim. Sin.*, 2010, **26**, 1761.

57 J.-B. Ma, X.-N. Wu, Y.-X. Zhao, X.-L. Ding and S.-G. He, *Chin. J. Chem. Phys.*, 2010, **23**, 133.

58 Z.-C. Wang, X.-N. Wu, Y.-X. Zhao, J.-B. Ma, X.-L. Ding and S.-G. He, *Chem.–Eur. J.*, 2011, **17**, 3449.

59 W. Xue, S. Yin, X.-L. Ding, S.-G. He and M.-F. Ge, *J. Phys. Chem. A*, 2009, **113**, 5302.

60 S. Yin, W. Xue, X.-L. Ding, W.-G. Wang, S.-G. He and M.-F. Ge, *Int. J. Mass Spectrom.*, 2009, **281**, 72.

61 H.-G. Xu, Z.-G. Zhang, Y. Feng, J. Y. Yuan, Y. C. Zhao and W. J. Zheng, *Chem. Phys. Lett.*, 2010, **487**, 204.

62 H.-B. Wu, S. R. Desai and L.-S. Wang, *J. Phys. Chem. A*, 1997, **101**, 2103.

63 H. Häkkinen, B. Yoon, U. Landman, X. Li, H.-J. Zhai and L.-S. Wang, *J. Phys. Chem. A*, 2003, **107**, 6168.

64 A. D. Becke, *Phys. Rev. A: At., Mol., Opt. Phys.*, 1988, **38**, 3098.

65 A. D. Becke, *J. Chem. Phys.*, 1993, **98**, 5648.

66 C. T. Lee, W. T. Yang and R. G. Parr, *Phys. Rev. B: Condens. Matter*, 1988, **37**, 785.

67 A. Schäfer, C. Huber and R. Ahlrichs, *J. Chem. Phys.*, 1994, **100**, 5829.

68 Y.-P. Ma, W. Xue, Z.-C. Wang, M.-F. Ge and S.-G. He, *J. Phys. Chem. A*, 2008, **112**, 3731.

69 H. B. Schlegel, *J. Comput. Chem.*, 1982, **3**, 214.

70 C. Gonzalez and H. B. Schlegel, *J. Chem. Phys.*, 1989, **90**, 2154.

71 C. Gonzalez and H. B. Schlegel, *J. Phys. Chem.*, 1990, **94**, 5523.

72 S. F. Boys and F. Bernardi, *Mol. Phys.*, 1970, **19**, 553.

73 S. Simon, M. Duran and J. J. Dannenberg, *J. Chem. Phys.*, 1996, **105**, 11024.

74 A. D. Becke, *J. Chem. Phys.*, 1996, **104**, 1040.

75 J. P. Perdew, K. Burke and M. Ernzerhof, *Phys. Rev. Lett.*, 1996, **77**, 3865.

76 T. van Voorhis and G. E. Scuseria, *J. Chem. Phys.*, 1998, **109**, 400.

77 A. D. Becke, *J. Chem. Phys.*, 1993, **98**, 1372.

78 C. Adamo and V. Barone, *Chem. Phys. Lett.*, 1997, **274**, 242.

79 J. P. Perdew and Y. Wang, *Phys. Rev. B: Condens. Matter*, 1991, **45**, 13244.

80 C. Lee, W. Yang and R. G. Parr, *Phys. Rev. B: Condens. Matter*, 1988, **37**, 785.

81 J. P. Perdew, K. Burke and M. Ernzerhof, *Phys. Rev. Lett.*, 1997, **78**, 1396.

82 J. P. Perdew, *Phys. Rev. B: Condens. Matter*, 1986, **33**, 8822.

83 N. B. Balabanov and K. A. Peterson, *J. Chem. Phys.*, 2005, **123**, 064107.

84 T. H. Dunning, Jr., *J. Chem. Phys.*, 1989, **90**, 1007.

85 K. Raghavachari, G. W. Trucks, J. A. Pople and M. Head-Gordon, *Chem. Phys. Lett.*, 1989, **157**, 479.

86 J. D. Watts, J. Gauss and R. J. Bartlett, *J. Chem. Phys.*, 1993, **98**, 8718.

87 M. J. Frisch, G. W. Trucks, H. B. Schlegel, G. E. Scuseria, M. A. Robb, J. R. Cheeseman, J. A. Montgomery, Jr., T. Vreven, K. N. Kudin, J. C. Burant, J. M. Millam, S. S. Iyengar, J. Tomasi, V. Barone, B. Mennucci, M. Cossi, G. Scalmani, N. Rega, G. A. Petersson, H. Nakatsuji, M. Hada, M. Ehara, K. Toyota, R. Fukuda, J. Hasegawa, M. Ishida, T. Nakajima, Y. Honda, O. Kitao, H. Nakai, M. Klene, X. Li, J. E. Knox, H. P. Hratchian, J. B. Cross, V. Bakken, C. Adamo, J. Jaramillo, R. Gomperts, R. E. Stratmann, O. Yazyev, A. J. Austin, R. Cammi, C. Pomelli, J. Ochterski, P. Y. Ayala, K. Morokuma, G. A. Voth, P. Salvador, J. J. Dannenberg, V. G. Zakrzewski, S. Dapprich, A. D. Daniels, M. C. Strain, O. Farkas, D. K. Malick, A. D. Rabuck, K. Raghavachari, J. B. Foresman, J. V. Ortiz, Q. Cui, A. G. Baboul, S. Clifford, J. Cioslowski, B. B. Stefanov, G. Liu, A. Liashenko, P. Piskorz, I. Komaromi, R. L. Martin, D. J. Fox, T. Keith, M. A. Al-Laham, C. Y. Peng, A. Nanayakkara, M. Challacombe, P. M. W. Gill, B. G. Johnson, W. Chen, M. W. Wong, C. Gonzalez and J. A. Pople, *GAUSSIAN 03 (Revision C.02)*, Gaussian, Inc., Wallingford, CT, 2004.

88 G. de Petris, A. Troiani, M. Rosi, G. Angelini and O. Ursini, *Chem.–Eur. J.*, 2009, **15**, 4248.

89 N. Dietl, M. Engeser and H. Schwarz, *Angew. Chem., Int. Ed.*, 2009, **48**, 4861.

90 W. Xue, Z.-C. Wang, S.-G. He, Y. Xie and E. R. Bernstein, *J. Am. Chem. Soc.*, 2008, **130**, 15879.

91 J. Roithová and D. Schröder, *Chem. Rev.*, 2010, **110**, 1170.

92 Y.-X. Zhao, X.-N. Wu, J.-B. Ma, S.-G. He and X.-L. Ding, *J. Phys. Chem. C*, 2010, **114**, 12271.

93 J.-B. Ma, X.-N. Wu, Y.-X. Zhao, X.-L. Ding and S.-G. He, *J. Phys. Chem. A*, 2010, **114**, 10024.

94 K. R. Asmis and J. Sauer, *Mass Spectrom. Rev.*, 2007, **26**, 542.

95 B. A. Arndtsen, R. G. Bergman, T. A. Mobley and T. H. Peterson, *Acc. Chem. Res.*, 1995, **28**, 154.

96 K.-M. Jeong and F. Kaufman, *J. Phys. Chem.*, 1982, **86**, 1808.

97 D. Schröder, S. Shaik and H. Schwarz, *Acc. Chem. Res.*, 2000, **33**, 139.

98 For example, an oxygen atom transfer reaction $^3Sc_3O_6^- + {}^1X \rightarrow {}^3Sc_3O_5^-$ (or $^1Sc_3O_5^-$) $+ {}^1XO$ will possibly involve spin triplet to singlet conversion because the ground state of $Sc_3O_5^-$ is a singlet (Fig. 3c).